Research Article

Adsorption Science & Technology
Volume 42: 1–18

DOI: 10.1177/02636174241254627
journals.sagepub.com/home/adt

Decoration of carbohydrate nanocomposite with silver nanoparticles for highly efficient adsorption of methylene blue and antimicrobial against human pathogens

Ahmed K. Saleh
Cellulose and Paper Department, National Research Centre, Giza, Egypt

Rasha Jame
Department of Chemistry, Faculty of Science, University of Tabuk, Tabuk, Kingdom of Saudi Arabia

Fatimah A. Alotaibi
Department of Chemistry, Faculty of Science, University of Tabuk, Tabuk, Kingdom of Saudi Arabia

Mahmoud A. Abdelaziz
Department of Chemistry, Faculty of Science, University of Tabuk, Tabuk, Kingdom of Saudi Arabia

Noha Omer
Department of Chemistry, Faculty of Science, University of Tabuk, Tabuk, Kingdom of Saudi Arabia

Abstract

The current study aims to prepare carbohydrate nanocomposite based on 2,2,6,6-tetramethylpiperidine-1-oxyl (TEMPO) oxidized cellulose nanofibers (CNFs) /chitosan chloride (Ch) decorated with silver nanoparticles (Ag-NPs) and designed as (TEMPO/CNF/Ch/Ag-NPs) that was investigated as antimicrobial materials and applied as efficient sorbent. CNF was prepared from cellulose through TEMPO oxidation-mechanical defibrillation technique. Anionic CNF and Ch were ironically interacted to prepare novel sustainable ionic nanofibers films. Ag-NPs having approximately

Submitted December 10, 2023; accepted April 2, 2024

Corresponding author:
Ahmed K. Saleh, Cellulose and Paper Department, National Research Centre, 33 El-Bohouth St, Dokki, P.O. 12622, Giza, Egypt
Email: asrk_saleh@yahoo.com

20 nm were prepared *in situ* to decorate the ionic fibers. The effects of experimental parameters including media pH (3.0–8.0), contact time (10–120 min), and initial methylene blue (MB) concentration (50–800 ppm) on the adsorption behavior of MB onto nanocomposite films were evaluated. The results exhibited similar and fast adsorption kinetic, as illustrated by the pseudo-second-order model. The adsorption results were best suited by the Langmuir isotherm model, and the maximum adsorption capacity for the TEMPO/CNF/Ch and TEMPO/CNF/Ch/Ag-NPs nanocomposite was 369 and 432 mg/g, respectively, at the optimized media pH of 7 with a contact time of 60 min at 88 to 90 mg/g of MB. In kinetic studies, the pseudo-second-order model for nanocomposite films provided the best fit ($R^2 = 0.98$), than pseudo-first-order model ($R^2 = 0.82$ and 0.77). The TEMPO/CNF/Ch and TEMPO/CNF/Ch/Ag-NPs nanocomposite retains 73 and 69% of its initial adsorption performance towards MB after five consecutive runs. The formed nanocomposite showed excellent efficacy against *Escherichia coli* (14.3 ± 0.57 mm), followed by *Candida albicans* (12 ± 1 mm), *Staphylococcus aureus* (11.3 ± 1.15 mm), and *Streptococcus mutans* (10.6 ± 1.15 mm), and their antimicrobial activity was enhanced by the incorporation of Ag-NPs. The formed nanocomposite might find applications in industrial and biomedical fields.

Keywords
cellulose nanofibers, silver nanoparticles, nanocomposite, adsorption, antimicrobial

Introduction

Wastewater remediation has become increasingly important in recent years for both purifying and reusing wastewater. Dye pollution is a serious threat to the environment, bringing severe environmental problems (El Boujaady et al., 2011). Several industries, such as fabrics, cosmetics, leathering, printing, and painting, use organic dyes, which are considered a major source of water pollution containing organic dyes (Safranin) (M Fayazi et al., 2015) and harmful organic pollutants (Rhodamine B) (Eslaminejad et al., 2023). Methylene blue (MB) is widely applied to chemical indicators, drugs, and biological stains. Before releasing dye-containing wastewater into water bodies or groundwater, MB must be removed from the industrial waste (Boukhemkhem and Rida, 2017; Jedynak and Repelewicz, 2017). Many problems result from the effluent of contaminated water without any treatment, such as decreasing water transparency and the oxygen transfer rate into the water (J. Singh and Dhaliwal, 2021). Wastewater dyes have recently been treated using several technologies and strategies (Abouzeid et al., 2018; Monier and Abdel-Latif, 2013). Owing to its high efficiency and economy, adsorption has gained considerable attention as a strategy for dye removal. It is therefore highly appropriate to develop cost-effective methods to eliminate organic dyes from effluents (Monier et al., 2010). Polysaccharides have attracted considerable interest as adsorbents and have been widely explored in various forms. Among the polysaccharides, cellulose is the most abundant naturally occurring polysaccharide, producing approximately 10^{12} tons annually from a variety of sources like plants, animals, and algae (Dai et al., 2021; Hadid et al., 2021; Zhang et al., 2017). In addition to being non-toxic, biodegradable, widely available, low-cost, and renewable, cellulose is widely used as a sustainable starting platform to prepare innovative adsorbents. Moreover, the compact structure of cellulose and the weak surface area generated by interchain H-bonds limit its application in the field of adsorption. Preparing new composites containing various organic and inorganic reagents is considered a promising technique for

improving the thermal stability, reactivity, and removal efficiency of polysaccharides. These approaches afford additional active locations at the adsorbent surface, which increases the removal efficiency of organic and inorganic pollutants from wastewater (Atta et al., 2013; Monier and Abdel-Latif, 2013). The oxidation of primary hydroxyl groups has been studied as an effective method to assist in the creation of new functional sites such as carboxylate groups, which promote strong electrostatic repulsion to assist cellulose defibrillation. Metal nanoparticles have recently been used as adsorbents because of their unique properties, such as high surface areas, controlled sizes, and highly reactive sites. For example, MoO3 nanorods (Moghazy, 2023), carbon nanotube (Ali et al., 2019), zinc oxide (Salehi et al., 2010), silver (Ag) (Abou-Zeid et al., 2019), and TiO_2-NPs (Owda et al., 2022) have proved to be more efficient and effective in water purification. Silver nanoparticles (Ag-NPs) have been described as an effective adsorbent for dyes. For example, crystal violet dye was effectively removed by Ag-NPs with a 97.2% removal efficiency (Satapathy et al., 2015). According to Azeez et al., biosynthesized Ag-NPs can remove Rhodamine B dye with 93% effectiveness (Azeez et al., 2018). Kasula et al. synthesized Ag metal organic frameworks for immobilization on and between GO sheets using an ultrasonication process to enhance their physicochemical properties. The adsorption capacities of Ag containing materials for MB were thoroughly evaluated at different experimental conditions (Kasula et al., 2022). Another study reported that bacterial cellulose functionalized with activated charcoal was used as a filtration system for MB removal (Saleh et al., 2021). In this study, cellulose was oxidized to form 2,2,6,6-tetramethylpiperidine-1-oxyl (TEMPO)/ cellulose nanofiber (CNF) which ionically interacted with cationic chitosan chloride (Ch) derivative to form ionic composite films. TEMPO/CNF/Ch films were decorated with Ag-NPs to improve their physical and adsorption behavior. The role of TEMPO/CNF which contains anionic carboxylate groups as well as the rich density of the hydroxyl groups are expected to contribute to the adsorption process. Moreover, immobilization of Ag-NPs may enhance the adsorption process for removing MB dye. Various optimization parameters such as contact time, dye concentration and solution pH on removal of MB efficiency were evaluated. Moreover, the kinetics and isotherms of the adsorption technique were recognized and evaluated via different mathematical models to evaluate the mechanism MB adsorption. Finally, the reusability of nanocomposite was calculated through desorption tests. The biological efficacy of the nanocomposite was tested against human pathogens including bacteria and yeast.

Experimental

Materials

Bagasse pulp was obtained from the Quena Paper Industry Company in Egypt. MB (12627-53-1) was supplied from SD Fine-Chem, Mumbai, India. Sodium hypochlorite (7681-52-9), TEMPO (2226-96-2) and sodium bromide (7647-15-6) were supplied from Sigma Aldrich, Saint Louis, USA. Silver nitrate (7761-88-8) was purchased from Alpha Chemika, Savgan Heights, India. Other chemicals were of analytical grade and used as received without further purification.

Preparation of TEMPO/CNF

TEMPO-oxidized CNF was prepared according to a previous study (Saito et al., 2011), with little change by dispersing 20 g of bagasse pulp in distilled water containing 0.8 g TEMPO and 0.8 g of sodium bromide. After adding 300 mL sodium hypochlorite solution (15%), the pH was adjusted to 10. The pH was lowered to 7.0 and the product was centrifuged and purified by dialysis against distilled water. The oxidized fibers were further defibrillated using Masuko grinder as mechanical defibrillation treatment. For calculating the

carboxylate content, 50 mg dried CNF was suspended in 0.01 M HCl (15 mL), deionized water, and titrated with standard NaOH. The carboxylate content, C (mmol/g), was calculated using Equation (1):

$$C = ((V_1 - V_o) \times C_{NaOH}) / m \quad (1)$$

Where (V_1) and (V_o) are the volumes of NaOH before and after titration, (C_{NaOH}) is the concentration of sodium hydroxide, and (m) is the weight of the dried CNF (A. Salama et al., 2020).

Decorated carbohydrate nanocomposite preparation

The nanocomposites were prepared according to the methods described by Almasi et al. with slight modifications (Almasi et al., 2018). In brief, TEMPO/CNF (0.3 g) was mixed with medium molecular weight Ch (degree of deacetylation, 75–85%) (0.3 g) with continuous stirring at 60°C for 4 h and poured into a Petri dish to prepare the TEMPO/CNF/Ch film. This film was immersed in an Ag nitrate solution (2 mM) which was prepared by dissolving 50 mL of Ag nitrate. After 6 h of gentile stirring, 2 mM glucose was gradually added to the suspension under continuous stirring at 80 °C for 4 h to achieve complete reduction. The synthesized TEMPO/CNF/Ch/Ag-NPs nanocomposite film was separated from the reaction medium and washed by deionized water and dried at 70 °C for preparing the nanocomposite film.

Characterization of samples

The characteristic functional groups of the CNF and nanocomposites were investigated using FT-IR (Mattson 5000 FTIR spectrometer) in the range of 4000–500 cm^{-1}. The morphology of the composites was determined using Model Quanta 250 FEG (Field Emission Gun) attached with EDX Unit (Energy Dispersive X-ray Analyses), with accelerating voltage 30 K. The internal structure of the CNFs and TEMPO/CNF/Ch/Ag-NPs nanocomposite was analyzed using a JEOL JEM-2100 electron microscopy at 100k × magnification, with an acceleration voltage of 120 kV. An X-ray diffractometer equipped with an automatic divergent slit Philips diffractometer (type PW 3710) was used. The patterns were run with Ni-filtered copper radiation (λ = 1.5404 Å) at 30 kV and 10 mA with a scanning speed of 2θ=2.5°/min.

Applications of decorated carbohydrate nanocomposite

Adsorption evaluation. The adsorption studies of MB were performed according to Pezoti Jr et al., 2014, with some changes. The adsorption behavior of TEMPO/CNF/Ch and TEMPO/CNF/Ch/Ag-NPs nanocomposite was studied via a batch technique. To investigate the adsorption efficiency, MB dye solution was prepared by dissolving 25 mg of the adsorbent in 50 mL dye solution in the dark at room temperature. The adsorption experiments were carried out in a 50 mL glass vials. Studying the effect of pH, contact time and initial concentration on the adsorption of MB was carried out. In brief, 25 mg of TEMPO/CNF/Ch and TEMPO/CNF/Ch/Ag-NPs nanocomposite were added into 50 mL of MB solutions, and the pH of the solution was adapted using HCl or NaOH solutions. The effect of the dye solution pH was investigated in the range from 3 to 8 and the pH at maximum adsorption efficiency was chosen as the maximum pH in the next experiments. Afterward, the effects of MB concentration (50−800 mg/L) and contact time (10−120 min) of the adsorption were investigated in batch experiments (pH = 7). After adsorption experiments at different times and concentrations, the supernatants were removed through centrifugation. Samples of 3 ml were taken from the solution, and the MB concentrations were calculated via UV-visible spectrophotometry. Maximum adsorption capacity (q_e) is achieved according to equation (2).

$$q_e = \frac{(Ci - Co)V}{m} \quad (2)$$

Initial dye concentration (Ci) and equilibrium concentration (Co) are represented in mg/L. Moreover, V (L) signifies dye solution volume and m (g) is the film mass. At equilibrium, q_e is the maximum adsorption.

Antimicrobial activity

Human pathogens and media. Mueller Hinton broth media composed of (%): 0.2 beef extract, 1.75 acid hydrolysate of casein, and 0.15 starch were used for the cultivation of different human pathogenic microorganisms obtained from the American Type Culture Collection (ATCC) including Gram-negative bacteria *Escherichia coli* ATCC 25922 (*E. coli*) and *Salmonella typhimurium* ATCC 14028 (*S. typhimurium*), Gram-positive bacteria *Staphylococcus aureus* ATCC 25923 (*S. aureus*) and *Streptococcus mutans* ATCC 25175 (*S. mutans*), and yeast *Candida albicans* ATCC 10231 (*C. albicans*). All microbes were incubated for 1 day at 37 ^{o}C and agitated at 200 rpm for pre-inoculum preparation.

Agar well-diffusion technique. The antimicrobial activities of the TEMPO/CNF, TEMPO/CNF/Ch, and TEMPO/CNF/Ch/Ag-NPs nanocomposites were evaluated qualitatively using agar well-diffusion technique according to our previous work with little change (Saleh et al., 2022). First, all the samples were dispersed in dimethyl sulfoxide (DMSO) at a concentration of 0.04 mg/mL. Approximately 15 mL of sterilized Mueller Hinton media (20 g/L agar) was poured onto a Petri dish and allowed to solidify. The microbial suspension (10^8 CFU/mL) with approximately equal concentration or density to 0.5 McFarland standards was spread on a Petri dish. Four wells (5 mm in diameter) were made with the solidified media using a sterile glassy borer and loaded with 70 µL of the tested samples. The negative control was prepared by loading one well with DMSO. All the plates were first incubated at 4 °C for 2 h to complete the diffusion of the tested sample and temporarily inhibit the model microbes, and subsequently incubated at 37 °C for 1 day. The zones of inhibition were estimated by measuring the diameter of the microbial growth inhibition zones (including the wells). Values are the average of three independent experiments.

Results and discussion

XRD, Ft-Ir, and TEM analysis of TEMPO/CNF

Bagasse residue was reported as an important source of CNF (El-Sayed et al., 2022). It contained 69.23% alpha-cellulose, 29% pentosan, 0.92% lignin, and 0.85% ash, as reported in our previous study (A. Salama et al., 2020). We propose the use of TEMPO-mediated oxidation to convert the hydroxyl groups within the D-glucose units at C6 into charged carboxyl entities, which enables the selective oxidation of the hydroxymethyl groups of cellulose. In this method, only a low degree of oxidation can be achieved, because intramolecular hydrogen bonds cannot alter the crystal structure of cellulose, providing only surface oxidation. After oxidation, the carboxylate content reached 1.44 mmol/g. XRD pattern reported in Figure 1a exhibits diffraction peaks at 16.4 and 23.1^{o} that refer to (110) and (200), typical of neat cellulose. The peak observed at approximately 34° can be attributed to the (004) plane. The CI values of the samples were determined according to Segal et al. (Segal et al., 1959), using the following equation:

$$\text{C.I.}(\%) = \frac{I_{002} - I_{am}}{I_{002}} \times 100 \quad (3)$$

Wherein I_{002} is the intensity of diffraction peak of (002) lattice plane, and I_{am} is the intensity of the amorphous background scatter measured. The C.I.(%) of TEMPO/CNF was 68%, while another study reported that the C.I of TEMPO/CNF was at 75% (Kamel et al., 2020). After the TEMPO oxidation process, FT-IR spectroscopy revealed an additional

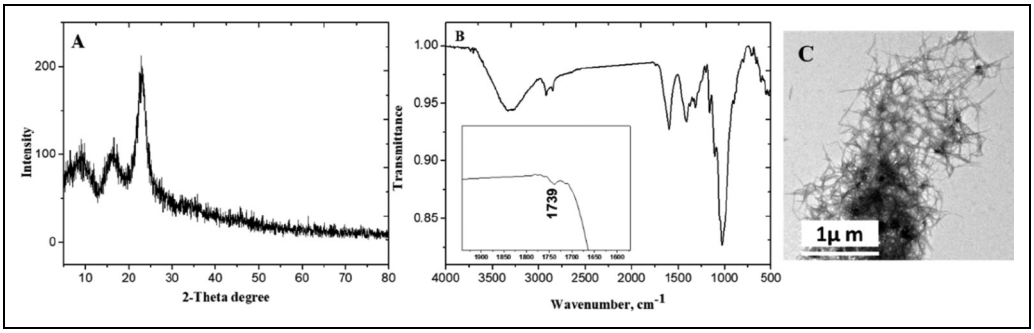

Figure 1. Characterization of TEMPO/CNF film by XRD pattern (a), FT-IR spectra (b), and TEM analysis (c). TEMPO: 2,2,6,6-tetramethylpiperidine-1-oxyl; CNF: cellulose nanofiber.

band at 1739cm^{-1}, attributed to the stretching of carbonyl groups, which further supports the oxidation process, as shown in Figure 1b. The internal structure of TEMPO/CNF was observed using TEM analysis which exhibited uniform sizes (a few micrometers in length and diameters varying from 5 to 12 nm) as shown in Figure 1c. According to previous studies, TEMPO/CNF networks have a uniform structure, because carboxylate groups are created homogeneously on their surfaces (A. Salama and Abou-Zeid, 2021).

XRD and Ft-Ir of decorated carbohydrate nanocomposite

The FT-IR spectra of TEMPO/CNF/Ch and TEMPO/CNF/Ch/Ag-NPs nanocomposites are illustrated in Figure 2 (left). The two composites displayed distinctive bands at approximately 3450 cm^{-1} which were assigned to OH stretching vibrations. The FT-IR spectra of the TEMPO/CNF/Ch/Ag-NPs nanocomposite were very close to those of TEMPO/CNF/Ch. However, a shoulder peak at 1649 cm^{-1} appeared for the TEMPO/CNF/Ch/Ag-NPs nanocomposite which may indicate the occurrence of chemical interactions with the amine groups. The absorption band at 1649 cm^{-1} confirmed the presence of carbonyl groups in the CNF (Pottathara et al., 2020). The XRD pattern confirmed the incorporation of the synthesized Ag-NPs into TEMPO/CNF/Ch. Figure 2 (right) shows the peaks of the Ag-NPs at 32.4 and 46.5^{o} which were assigned to the main (111) and (220) crystallographic planes of face-centered cubic (fcc) Ag crystals (JCPDS 00–004-0783). As no peaks were detected for any other phase, single-phase Ag-NPs with a cubic structure were obtained directly (Chandran et al., 2006).

SEM and TEM examination of decorated carbohydrate nanocomposite

The morphology of the TEMPO/CNF/Ch/Ag-NPs nanocomposite was examined by SEM at different magnifications, as shown in Figure 3a and b. The SEM micrograph showed a wrinkled surface. There was intertwining of the particles, resulting in a microstructure that was slightly dense and smooth. White particles appeared on the surface of the nanocomposite films indicating successful *in situ* synthesis of Ag-NPs as the same observations reported by (Boonpavanitchakul et al., 2020; Wang et al., 2022). This structure can enhance the chances of contact with organic molecules and improve the adsorption capacity of the nanocomposite. The EDX spectrum (Figure 3d) shows characteristic peaks related to cellulose and Ch derivatives (Carbon, Oxygen and Nitrogen). Furthermore, EDX analysis of the TEMPO/CNF/Ch/Ag-NPs nanocomposite showed the presence of Ag element which proves the incorporation of Ag-NPs

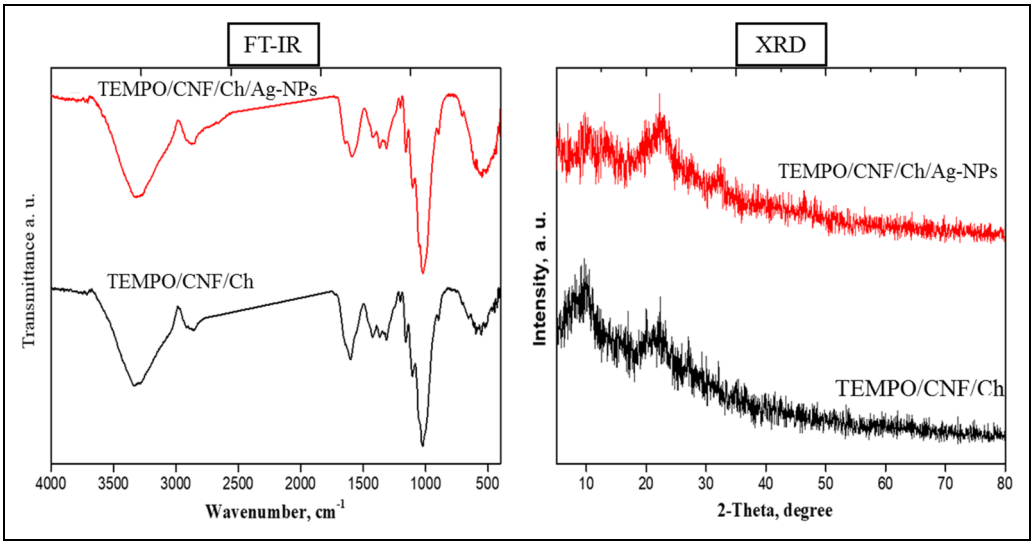

Figure 2. FT-IR spectroscopy and XRD analysis of TEMPO/CNF/Ch and TEMPO/CNF/Ch/Ag-NPs nanocomposite film. TEMPO: 2,2,6,6-tetramethylpiperidine-1-oxyl; CNF: cellulose nanofiber; Ch: chitosan chloride; Ag-NPs: silver nanoparticles.

into TEMPO/CNF/Ch (Chinthalapudi et al., 2021). Ag-NPs generally show a typical optical absorption peak approximately at 3 keV due to surface plasmon resonance as reported by (Chinthalapudi et al., 2021; Vijayakumar et al., 2024). Ag-NPs can be studied by TEM for their morphology and size details. Figure 3c represents the TEM image of the colloidal TEMPO/CNF/Ch/Ag-NPs composite which exhibits uniform particle diameter distribution of Ag-NPs (~ 20 nm). These results prove the crucial role of ionic polysaccharides for controlling the size of Ag-NP during the reducing of Ag^{+} to Ag0 (A. Salama, 2017).

Applications of decorated carbohydrate nanocomposite

Adsorption of methylene blue. To highlight the usefulness of functionalized polysaccharides derivatives, TEMPO/CNF/Ch film was examined with MB dye as a model for cationic organic pollutants. Moreover, the TEMPO/CNF/Ch/Ag-NPs nanocomposite was also tested to evaluate the influence of surface decoration with Ag-NPs. Therefore, MB adsorption was investigated in relation to different factors.

Effect of pH. As pH affects the binding sites of the adsorbent, it plays vital role in the ability of any adsorbent to remove organic dyes. The effect of pH was examined on TEMPO/CNF/Ch and TEMPO/CNF/Ch/Ag-NPs nanocomposite to evaluate their adsorption efficiency. The data showed that the adsorption efficiency of the examined TEMPO/CNF/Ch toward MB molecules increased sharply from 45 mg/g to 88 mg/g by increasing the pH from 3 to 7, these results are in agreement with other report study (Chinthalapudi et al., 2021). The low adsorption efficiency observed at acidic conditions may be attributed to the competitive interactions between protons and the cationic MB molecules. According to Maryam Fayazi and Rezvannejad, when the pH is raised from 2.0 to 6.0, the sepiolite clay/Ag-NPs nanocomposite shows an adsorption effectiveness of MB from 30.5 to 95.4% and subsequently plateaus

at a higher pH value (Maryam Fayazi and Rezvannejad, 2024).Also, the results related to the effect of pH on the MB adsorption by TEMPO/CNF/Ch/Ag-NPs nanocomposite are presented in Figure 4. Negative charge density of films increases with high pH because of the presence of OH^- ions on their surface. Additionally, the carboxylic groups are deprotonated and form COO^- groups, leading to efficient adsorption properties for MB (Zhao et al., 2022). The increased adsorption capacity of TEMPO/CNF/Ch/Ag-NPs nanocomposite may be due to the large specific surface area and surface energy of incorporated Ag-NPs inside the polymer film (J. Singh and Dhaliwal, 2021). The zero-charge point (pHpzc) of Ag-NPs and the pKa value of MB are 7.82 and 3.8, respectively. At higher pH than pHpzc, owing to deprotonation on the surface of the Ag-NPs, negative charge distribution appears. At a pH lower than pHpzc, protonation distributes the positive charge on the Ag-NPs. As a result, at acidic pH, the repulsion force between positive charges on the TEMPO/CNF/Ch/Ag-NPs nanocomposite surface and positively charged MB reduce the adsorption efficiency. However, at alkaline pH, the negatively charged Ag-NPs interact with the positively charged MB molecules increasing adsorption efficiency (Yari et al., 2021).

Effect of contact time and kinetics. Calculating the adsorption capacity of TEMPO/CNF/Ch and TEMPO/CNF/Ch/Ag-NPs nanocomposite is essential to estimate the adsorption equilibrium. Figure 5 displays that the adsorption capacity of MB onto TEMPO/CNF/Ch and TEMPO/CNF/Ch/Ag-NPs nanocomposite at different times increases rapidly at the initial stage. TEMPO/CNF/Ch recorded an adsorption efficiency of 88 mg/g, representing an MB equilibrium after 60 min. Saleh et al. reported that the equilibrium contact time was optimized to be 60 min when using modified bacterial cellulose with magnetite for the adsorption of methyl orange (Saleh et al., 2023). However, when TEMPO/CNF/Ch was decorated with Ag-NPs to prepare the TEMPO/CNF/Ch/Ag-NPs nanocomposite, the adsorption capacity improved to 90 mg/g. This result indicates that the decoration of TEMPO/CNF/Ch with Ag-NPs enhanced the adsorption capacity. Chinthalapudi et al. reported that the CNF/Ag-NPs nanocomposite affinity increased the adsorption efficacy of malachite green continuously by increasing the contact time until 100 min. After this time, the rate of adsorption is equal to that of desorption (Chinthalapudi et al., 2021). From results we can observe that up to 60 min, the adsorption efficiency of MB increased continuously and henceforth remained constant. This is due to the MB get adsorbed onto the Ag-NPs as time progresses. After a several time, there will be no vacant sites for the MB to occupy. At this time, the rate of adsorption is equal to that of desorption and the process is said to have attained the state of dynamic equilibrium. The equilibrium contact time was observed to be 60 min.

The adsorption kinetics of MB by TEMPO/CNF/Ch and TEMPO/CNF/Ch/Ag-NPs nanocomposites were calculated by fitting experimental values to pseudo-first-order, pseudo-second-order, and Elovich kinetic models (Table 1). The following equations (4), (5), and (6) represent the three kinetic models, respectively, which were developed to study the adsorption process of MB.

$$\log\,(q_e\,-\,q_t) = \log(q_e) - \frac{K_1}{2.303}\,t \quad (4)$$

$$\frac{t}{q_t} = \frac{t}{q_e} + \frac{1}{K_2 q_e^2} \quad (5)$$

$$q_t = \frac{1}{\beta}\,lin(\alpha\beta) + \frac{1}{\beta}\,ln\,t \quad (6)$$

Where q_e and qt (mg/g) are the capacity of adsorbed MB on the adsorbent at equilibrium and at time t (min). Also, K_1 and K_2 are the equilibrium rate constants of these models, while α and β represent the initial adsorption rate and the desorption constant, respectively. According to the fitting curves to the pseudo-first-order and the pseudo-second-order models

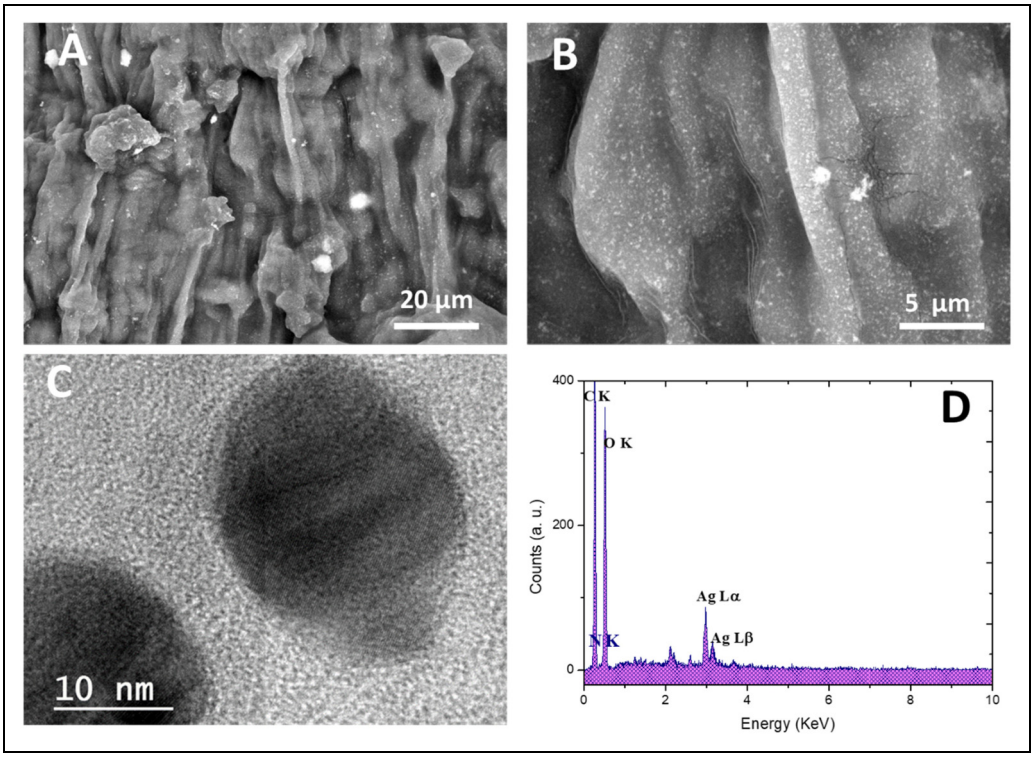

Figure 3. Characterization of TEMPO/CNF/Ch/Ag-NPs nanocomposite film by SEM at different magnifications (a, b), TEM analysis (c), and EDX (d). TEMPO: 2,2,6,6-tetramethylpiperidine-1-oxyl; CNF: cellulose nanofiber; Ch: chitosan chloride; Ag-NPs: silver nanoparticles.

for TEMPO/CNF/Ch and TEMPO/CNF/Ch/Ag-NPs nanocomposites, all the values of the correlation coefficient of the TEMPO/CNF/Ch and TEMPO/CNF/Ch/Ag-NPs nanocomposite are much higher for the pseudo-second-order model ($R^2 = 0.98$ for the two adsorbent) than pseudo-first-order model ($R^2 = 0.82$ and 0.77) as shown in the Table 1. The results presented in the adsorption study fit well with the pseudo-second-order model, showing a rate-limiting step that was facilitated by chemical reaction. A valence force interaction occurs by sharing electrons between MB molecules and the surface of the adsorbent. Although the plots of different initial MB concentrations do not cross the origin of an axis, it suggests that the adsorption method was also affected by mass transfer in addition to intraparticle diffusion. The pseudo-second-order constant, labeled k2, is 4.4×10^{-4} and 4.3×10^{-4} g mg^{-1} min^{-1} for TEMPO/CNF/Ch and TEMPO/CNF/Ch/Ag-NPs nanocomposite, respectively. Results show that MB is adsorbed via chemisorption onto TEMPO/CNF/Ch/Ag-NPs nanocomposite. A chemical adsorption process is described by the Elovich model when the adsorbing surface is heterogeneous and has different activation energies. This model has been used to describe many chemisorption adsorptions processes (R. Singh et al., 2021). The Elovich model for TEMPO/CNF/Ch showed $R^2 > 0.9$. A decrease in the value of β (a factor related to surface coverage) with the corresponding increase in α (adsorption rate) as MB increase proposes ion exchange as an appropriate adsorption mechanism.

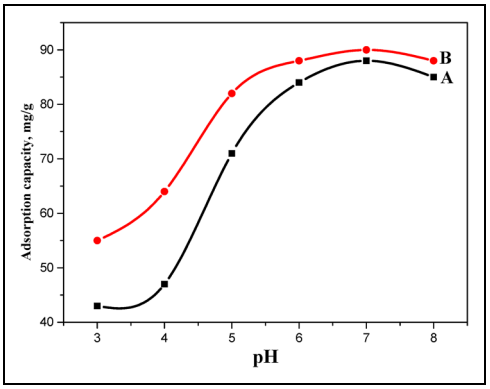

Figure 4. Effect of pH values on the adsorption capacities of TEMPO/CNF/Ch (a) and TEMPO/CNF/Ch/Ag-NPs (b) nanocomposite films towards Mb. TEMPO: 2,2,6,6-tetramethylpiperidine-1-oxyl; CNF: cellulose nanofiber; Ch: chitosan chloride; Ag-NPs: silver nanoparticles; MB: methylene blue.

Effect of MB concentration and equilibrium isotherm. With batches containing different MB concentrations (50–800 mg/L), MB dye was removed by increasing the initial concentration in both sorbents, as shown in Figure 6. Nevertheless, the TEMPO/CNF/Ch/Ag-NPs nanocomposite demonstrated higher capacity than the TEMPO/CNF/Ch, indicating the developed Ag-NPs significance in generating more attraction sites with the organic dye. The plot reveals that as the initial concentration of MG dye increases from 50 to 500 mg/L, the MB uptake by TEMPO/CNF/Ch and TEMPO/CNF/Ch/Ag-NPs nanocomposite increased in an almost linear fashion, after that the percentage adsorption of MB steady (Yagub et al., 2014). The adsorption isotherm was investigated for the two prepared samples. The adsorption capacity at equilibrium showed a fast increase at low initial MB concentrations and then developed steadily due to the occupation of active sites on TEMPO/CNF/Ch and TEMPO/CNF/Ch/Ag-NPs nanocomposite. The equilibrium of MB adsorption was examined by fitting the results to three adsorption isotherms Langmuir, Freundlich, and Temkin models.

The obtained isotherms were examined using the Langmuir model as represented by Equation (7).

$$\frac{C_e}{q_e} = \frac{K_s}{q_{\max}} + \frac{C_e}{q_{\max}} \tag{7}$$

Where Ce is the equilibrium concentration of the MB (mg/L); q_e is the adsorbed MB (mg/g) by either TEMPO/CNF/Ch or TEMPO/CNF/Ch/Ag-NPs nanocomposite sorbent; and K_s represents Langmuir constant (mg/L). The experimental isotherms results are associated with the Langmuir model with a high correlation coefficient (R^2) presented in Figure 6 in the case of both TEMPO/CNF/Ch and TEMPO/CNF/Ch/Ag-NPs nanocomposite sorbents. A monolayer interaction of the MB molecules onto both sorbents surfaces was proposed. Moreover, the maximum capacities of TEMPO/CNF/Ch and TEMPO/CNF/Ch/Ag-NPs nanocomposite were 369 and 432 mg/L, respectively. Consequently, TEMPO/CNF/Ch/Ag-NPs nanocomposite sorbent displayed an almost higher capacity value. The results indicate decoration process role in enhancing the adsorption capacity of organic dyes. The active sites on TEMPO/CNF/Ch and TEMPO/CNF/Ch/Ag-NPs nanocomposite had equal affinity to MB. Nanoparticles typically adhere to Langmuir isotherms when adsorbing dye (Gowda et al., 2022).

The calculated isotherms were examined by Freundlich and Temkin models which are mathematically presented by Equations 8 and 9

$$\log q_e = \frac{1}{n}\log C_e + \log p \tag{8}$$

$$q_e = \frac{RT}{\beta} ln\, \alpha + \frac{RT}{\beta}\, ln\ C_e \tag{9}$$

P indicates the adsorption capacity (mg/g) and 1/n is an empirical parameter. B_T is the Temkin constants and $B_T = RT/\ \beta$(J/mol) and α Denotes Temkin's equilibrium binding constant (L/g), which corresponds to the binding energy at maximum. The linear coefficient of the Freundlich model was 0.87 and 0.83. Adsorption processes were not adequately described by this model of the TEMPO/CNF

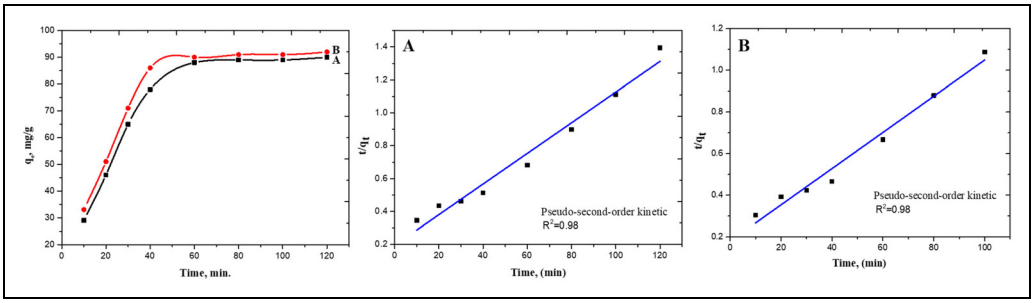

Figure 5. Effect of the incubation time on the adsorption capacity and kinetics appropriate to TEMPO/CNF/Ch (a) and TEMPO/CNF/Ch/Ag-NPs (b) nanocomposite film. TEMPO: 2,2,6,6-tetramethylpiperidine-1-oxyl; CNF; cellulose nanofiber; Ch: chitosan chloride; Ag-NPs: silver nanoparticles.

Table 1. Kinetic parameters for MB adsorption by TEMPO/CNF/Ch and TEMPO/CNF/Ch/Ag-NPs nanocomposite.

Models	Parameters	TEMPO/CNF/Ch	TEMPO/CNF/Ch/Ag-NPs
Pseudo-first-order	$q_{e,\ cal}$ (mg/g)	57	49
	K_1 (min^{-1})	0. 022	0.024
	R^2	0.82	0.77
Pseudo-second- order	$q_{e,\ cal}$ (mg/g)	108	114
	K_2 (g $mg^{-1}min^{-1}$)	4.4×10^{-4}	4.3×10^{-4}
	R^2	0.98	0.98
Elovich	α (mg·g·min^{-1})	9.22	12.26
	β (g·mg^{-1})	0.04	0.04
	R^2	0.92	0.88

TEMPO: 2,2,6,6-tetramethylpiperidine-1-oxyl; CNF: cellulose nanofiber; Ch: chitosan chloride; Ag-NPs: silver nanoparticles; MB: methylene blue.

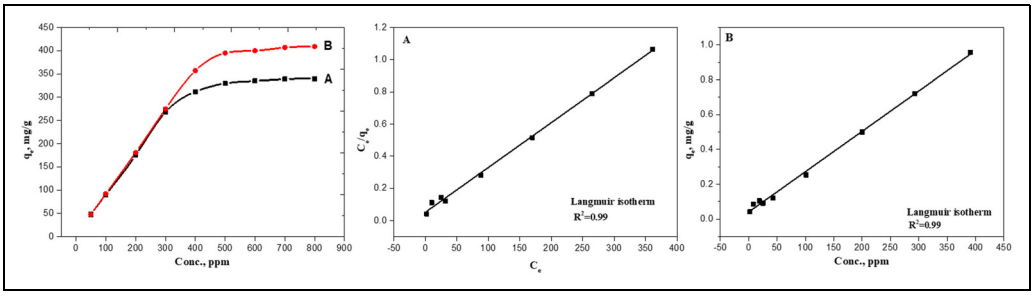

Figure 6. Effect of MB concentration on adsorption capacity and Langmuir adsorption isotherm models for TEMPO/CNF/Ch (a) and TEMPO/CNF/Ch/Ag-NPs (b) nanocomposite. TEMPO: 2,2,6,6-tetramethylpiperidine-1-oxyl; CNF: cellulose nanofiber; Ch: chitosan chloride; Ag-NPs: silver nanoparticles; MB: methylene blue.

Table 2. Parameters for MB adsorption by TEMPO/CNF and TEMPO/CNF/Ch/Ag-NPs nanocomposites.

Models	Parameters	TEMPO/CNF/Ch	TEMPO/CNF/Ch/Ag-NPs
Langmuir	q_m (mg g^{-1})	369	432
	K_s (L mg^{-1})	19.1	17.7
	R^2	0.99	0.99
Freundlich	P (mg/g)	47	52
	n	2.7	2.5
	R^2	0.84	0.81
Temkin	B_T (J mol^{-1})	64.4	77.5
	α (L mg^{-1})	0.13	0.87
	R^2	0.71	0.9

TEMPO: 2,2,6,6-tetramethylpiperidine-1-oxyl; CNF: cellulose nanofiber; Ch: chitosan chloride; Ag-NPs: silver nanoparticles; MB: methylene blue.

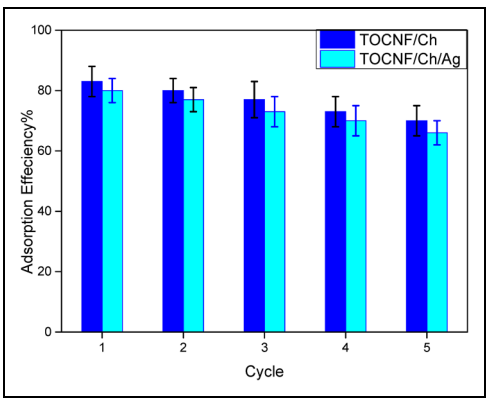

Figure 7. Adsorption–desorption cycles of MB for TEMPO/CNF/Ch and TEMPO/CNF/Ch/Ag-NPs nanocomposite. TEMPO: 2,2,6,6-tetramethylpiperidine-1-oxyl; CNF: cellulose nanofiber; Ch: chitosan chloride; Ag-NPs: silver nanoparticles; MB: methylene blue.

and TEMPO/CNF/Ch/Ag-NPs nanocomposite. The values of the Freundlich model constant *P (45 and 50)* and *n* (2.7 and 2.5) for TEMPO/CNF/Ch and TEMPO/CNF/Ch/Ag-NPs nanocomposite are presented in Table 2. Indirect adsorbate/adsorbate interactions are considered by the Temkin isotherm. Experiment data were not closely matched by the Temkin model (Wu and Andrews, 2020).

Adsorption mechanism. The adsorption process of MB by TEMPO/CNF/Ch and TEMPO/CNF/Ch/Ag-NPs nanocomposite had been proposed to be a monolayer chemical adsorption. The formation of carboxylic acid sodium salt in basic aqueous solutions was accompanied with the formation of negatively charged surface. Meantime, MB was ionized in the aqueous solution and positively charged due to the existence of tertiary amine. Thus, there was an electrostatic attraction interaction between the prepared two composites and MB during the adsorption process. Moreover, kinetics results exhibited the presence of chemical adsorption processes for MB dye onto TEMPO/CNF/Ch and TEMPO/CNF/Ch/Ag-NPs nanocomposite, further confirming the electrostatic interactions. Furthermore, the presence of various hydroxyl and amine groups on the surface of the composite may interact with the cationic MB dye via hydrogen bonding between the electronegative atoms (nitrogen and sulfur atoms) of MB dye and the functions groups of the adsorbent (Akhi et al., 2024). The Ag-NP may be reinforced within this composite matrix to improve the surface energy of the formed composite adsorbent to provide greater binding of MB dye. As a result, the adsorption performance was increased after Ag-NP incorporation.

Regeneration experiments. The MB-loaded TEMPO/CNF/Ch/Ag-NPs nanocomposite sorbent was activated utilizing HCl solution and recovered with an MB solution for several repeated uptake regenerations, and the maximum efficiency was evaluated. The TEMPO/CNF/Ch and TEMPO/CNF/Ch/Ag-NPs nanocomposite sustains around 73 and 69%, respectively, of its initial efficiency by the end of the fifth cycle, as shown in Figure 7. These outcomes indicate that the prepared nanocomposites are a stable adsorbent for MB adsorption. There are several studies that report the reusability of nanocomposite based on Ag-NPs for MB adsorption, such as

Table 4. Antimicrobial activity of the TEMPO/CNF, TEMPO/CNF/Ch and TEMPO/CNF/Ch/Ag-NPs nanocomposite against five pathogenic microbes.

Organism	Diameters of inhibition zone (mm)			
	DMSO	TEMPO/CNF	TEMPO/CNF/Ch	TEMPO/CNF/Ch/Ag-NPs
E. coli	0.0 ± 0.0^{c}	0.0 ± 0.0^{c}	10 ± 1^{a}	14.3 ± 0.57^{a}
S. typhimurium	0.0 ± 0.0^{c}	0.0 ± 0.0^{c}	0.0 ± 0.0^{c}	0.0 ± 0.0^{c}
S. aureus	0.0 ± 0.0^{c}	0.0 ± 0.0^{c}	8 ± 1^{b}	11.3 ± 1.15^{b}
S. mutans	0.0 ± 0.0^{c}	0.0 ± 0.0^{c}	7 ± 1^{b}	10.6 ± 1.15^{b}
C. albicans	0.0 ± 0.0^{c}	0.0 ± 0.0^{c}	11.6 ± 0.57^{a}	12 ± 1^{b}

Note: Statistical significance was indicated alphabetically (in descending significance order where $^{a} > ^{b} > ^{c}$, etc.) according to ANOVA analysis with CoStat program using least significant difference test (LSD) at p-value ≤ 0.05.
TEMPO: 2,2,6,6-tetramethylpiperidine-1-oxyl; CNF: cellulose nanofiber; Ch: chitosan chloride; Ag-NPs: silver nanoparticles; DMSO: dimethyl sulfoxide.

Table 3. Maximum adsorptions of MB using different composites.

Adsorbent	Maximum adsorption (mg/g)	References
TEMPO/CNF/Ch/Ag-NPs nanocomposite	432	The current study
Ch/silica nanocomposite	848	(A. Salama and Abou-Zeid, 2021)
Alginate/gelatin hydrogel/Ag-NPs nanocomposite	625	(Abou-Zeid et al., 2019)
TEMPO-oxidized cellulose coupled with 3-aminopropyl sulfonic acid	526	(El-Sayed et al., 2022)
TEMPO/CNF/graphene nanocomposite	227	(Hussain et al., 2018)
Cellulose/silk fibroin/calcium phosphate biocomposite	172	(A. Salama, 2020)
Copper/sodium alginate/activated carbon	86.96	(Maryam Fayazi, 2022)
Sepiolite clay/Ag-NPs	101.0	(Maryam Fayazi and Rezvannejad, 2024)

TEMPO: 2,2,6,6-tetramethylpiperidine-1-oxyl; CNF: cellulose nanofiber; Ch: chitosan chloride; Ag-NPs: silver nanoparticles; MB: methylene blue.

polystyrene-divinylbenzene/Ag-NPs, resulting in an adsorption ratio of 97.12% after five cycles (Xu et al., 2023), $Fe_3O_4/mTiO_2$/Ag-NPs core-shell, resulting in a removal ratio of MB of 98.7% after five cycles (Wen and Li, 2023).

As compared to other adsorbents based on polysaccharide modified adsorbents, TEMPO/CNF/Ch/Ag-NPs nanocomposite has efficiently adsorption capacities for MB absorption (Table 3).

Antimicrobial against human pathogens. The antimicrobial effects of TEMPO/CNF, TEMPO/CNF/Ch, and TEMPO/CNF/Ch/Ag-NPs nanocomposite were explored on human pathogens using the agar well-diffusion technique. Significant inhibition zones were observed for the TEMPO/CNF/Ch and TEMPO/CNF/Ch/Ag-NPs nanocomposite against all tested microorganisms except *S. typhimurium*, as shown in Table 4 and Figure 8. The TEMPO/CNF/Ch film exhibited greater antimicrobial efficacy against *C. albicans* compared to *E. coli* and did not show significant effects against other tested microbes. This finding can be attributed to the presence of amine groups

in the Ch chain, which leads to an increase in the cationic charges. This results in an increased affinity for negatively charged components located on the surface of microbial cells, which in turn inhibits their biosynthesis, disrupts mass transport across the cell wall, and accelerates the death of the microbes (Li et al., 2013). The TEMPO/CNF/Ch/Ag-NPs nanocomposite demonstrates a greater degree of sensitivity towards E. coli than the other microbes utilized, with no significant differences observed. These findings are consistent with other studies (H. E. Salama et al., 2018; Yang et al., 2023). Because Ag-NPs are included in the composite, the TEMPO/CNF/Ch/Ag-NPs nanocomposite has significantly higher antimicrobial activity than TEMPO/CNF/Ch nanocomposite; this in agreement with other report study (Yahia et al., 2022). Several mechanisms may account for the antimicrobial activity of TEMPO/CNF/Ch/Ag-NPs. (A) Ag-NPs alter the membrane permeability of microbes by adhering to their surfaces. (B) Ag-NPs eliminate microbial cells by causing DNA damage (Khan et al., 2023; Vasylechko et al., 2017). (C) Disrupt the microbial function through interactions between Ag ions and thiol-containing proteins in the cell wall. In contrast, the effect of TEMPO/CNF and DMSO against all microbial pathogens was negligible (El-Gendi et al., 2023).

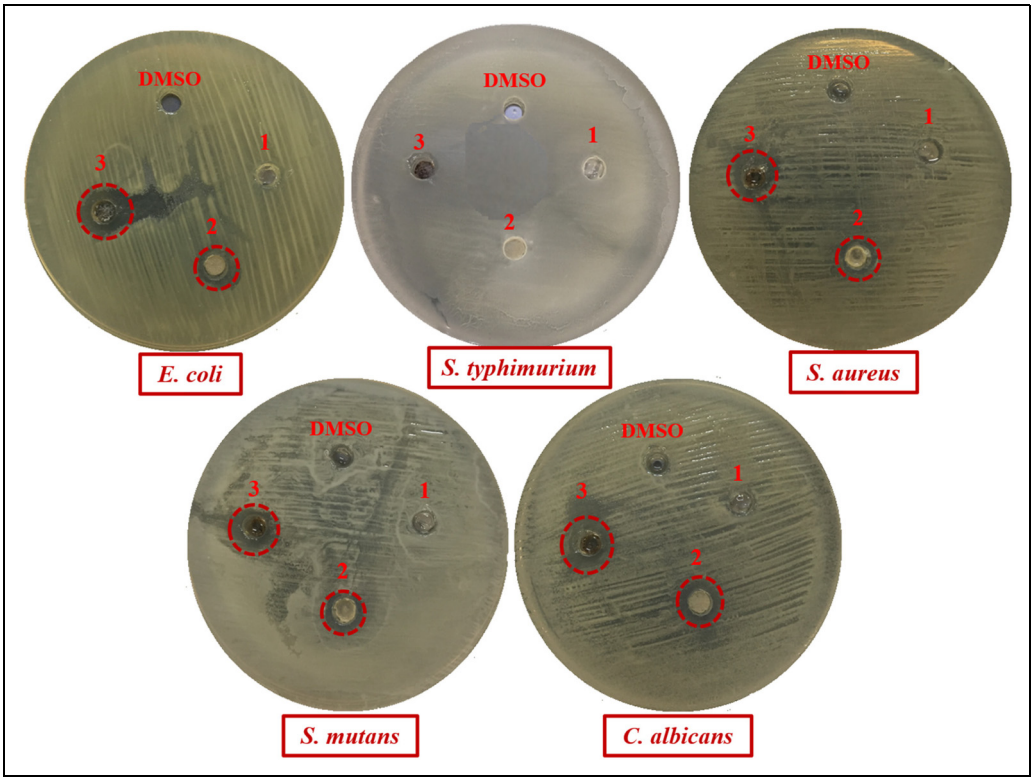

Figure 8. Antimicrobial evaluation expressed as halo-zones of TEMPO/CNF, TEMPO/CNF/Ch and TEMPO/CNF/Ch/Ag-NPs nanocomposite film labeled as 1, 2, and 3, respectively, with DMSO as negative control against five pathogenic microbes. TEMPO: 2,2,6,6-tetramethylpiperidine-1-oxyl; CNF: cellulose nanofiber; CNF: cellulose nanofiber; Ch: chitosan chloride; Ag-NPs: silver nanoparticles; DMSO: dimethyl sulfoxide.

Conclusion

In summary, the novelty of the current study was summarized in the oxidation of the obtained cellulose to prepare TEMPO/CNF which ionically interacts with cationic Ch derivative to form ionic composite films. TEMPO/CNF/Ch films were decorated with Ag-NPs to improve their physical, biological, and adsorption behavior. The morphological investigation, crystal phase, and chemical structure of the obtained nanocomposite film were evaluated by SEM, EDX, TEM, XRD, and FT-IR spectroscopy. Various parameters such as media pH, contact time, and MB concentration were evaluated for enhancing the adsorption process, and their optimal values were found to be 7, 60 min, and 88 to 90 mg/g, respectively, to achieve the adsorption capacity from 369 to 432 mg/g. Both the pseudo-second-order model and the Langmuir isotherm model appropriate the obtained results well, demonstrating a mutual affinity between TEMPO/CNF/Ch/Ag-NPs nanocomposite and MB molecules by chemical interaction. TEMPO/CNF/Ch/Ag-NPs nanocomposite demonstrated excellent adsorption capacity (432 mg/g) for MB. TEMPO/CNF/Ch/Ag-NPs nanocomposite demonstrated potent antibacterial activity against Gram-negative (except *S. typhimurium*) and Gram-positive bacteria and ant-yeast activity (*C. albicans*). The results revealed that the tested nanocomposite has two mechanisms of action for antimicrobial activity, due to the presence of Ag-NPs. The study demonstrates how enhancing ionic polysaccharides with Ag-NPs can improve antimicrobial and sorption performance.

Data availability

Data will be made available on request.

Declaration of conflicting interests

The authors declared no potential conflicts of interest with respect to the research, authorship, and/or publication of this article.

Funding

The authors received no financial support for the research, authorship, and/or publication of this article.

ORCID iD

Ahmed K. Saleh https://orcid.org/0000-0002-4711-8693

References

Abou-Zeid RE, Awwad NS, Nabil S, et al. (2019) Oxidized alginate/gelatin decorated silver nanoparticles as new nanocomposite for dye adsorption. *International Journal of Biological Macromolecules* 141(1): 1280–1286.

Abouzeid RE, Khiari R, El-Wakil N, et al. (2018) Current state and new trends in the use of cellulose nanomaterials for wastewater treatment. *Biomacromolecules* 20(2): 573–597.

Akhi AA, Hasan A, Saha N, et al. (2024) Ophiorrhiza mungos-mediated silver nanoparticles as effective and reusable adsorbents for the removal of methylene blue from water. *ACS omega* 9(4): 4324–4338.

Ali S, Rehman SAU, Luan HY, et al. (2019) Challenges and opportunities in functional carbon nanotubes for membrane-based water treatment and desalination. *Science of the Total Environment* 646(1): 1126–1139.

Almasi H, Jafarzadeh P and Mehryar L (2018) Fabrication of novel nanohybrids by impregnation of CuO nanoparticles into bacterial cellulose and chitosan nanofibers: Characterization, antimicrobial and release properties. *Carbohydrate Polymers* 186(15): 273–281.

Atta A, Akl MA, Youssef AM, et al. (2013) Superparamagnetic core-shell polymeric nanocomposites for efficient removal of methylene blue from aqueous solutions. *Adsorption Science & Technology* 31(5): 397–419.

Azeez L, Lateef A, Adebisi SA, et al. (2018) Novel biosynthesized silver nanoparticles from cobweb as adsorbent for rhodamine B: Equilibrium isotherm, kinetic and thermodynamic studies. *Applied Water Science* 8(32): 1–12.

Boonpavanitchakul K, Pimpha N, Kangwansupamonkon W, et al. (2020) Processing and antibacterial

application of biodegradable sponge nanocomposite materials of silver nanoparticles and silk sericin. *European Polymer Journal* 130(5): 109649.

Boukhemkhem A and Rida K (2017) Improvement adsorption capacity of methylene blue onto modified tamazert kaolin. *Adsorption Science & Technology* 35(9-10): 753–773.

Chandran SP, Chaudhary M, Pasricha R, et al. (2006) Synthesis of gold nanotriangles and silver nanoparticles using aloevera plant extract. *Biotechnology Progress* 22(2): 577–583.

Chinthalapudi N, Kommaraju VVD, Kannan MK, et al. (2021) Composites of cellulose nanofibers and silver nanoparticles for malachite green dye removal from water. *Carbohydrate Polymer Technologies and Applications* 2(25): 100098.

Dai H, Chen Y, Ma L, et al. (2021) Direct regeneration of hydrogels based on lemon peel and its isolated microcrystalline cellulose: Characterization and application for methylene blue adsorption. *International Journal of Biological Macromolecules* 191(30): 129–121.

El-Gendi H, Salama A, El-Fakharany EM, et al. (2023) Optimization of bacterial cellulose production from prickly pear peels and its ex situ impregnation with fruit byproducts for antimicrobial and strawberry packaging applications. *Carbohydrate Polymers* 302(15): 120383.

El-Sayed NS, Salama A and Guarino V (2022) Coupling of 3-aminopropyl sulfonic acid to cellulose nanofibers for efficient removal of cationic dyes. *Materials* 15(19): 6964.

El Boujaady H, El Rhilassi A, Bennani-Ziatni M, et al. (2011) Removal of a textile dye by adsorption on synthetic calcium phosphates. *Desalination* 275(1–3): 10–16.

Eslaminejad S, Rahimi R and Fayazi M (2023) Sepiolite-metal organic framework-iron oxide catalyst for degradation of rhodamine B using fenton-like process. *Journal of the Taiwan Institute of Chemical Engineers* 152(1): 105181.

Fayazi M (2022) Adsorption of methylene blue from aqueous media using carbon-alginate granules. *Environment and Water Engineering* 8(4): 765–777.

Fayazi M, Afzali D, Taher M, et al. (2015) Removal of safranin dye from aqueous solution using magnetic mesoporous clay: Optimization study. *Journal of Molecular Liquids* 212(1): 675–685.

Fayazi M and Rezvannejad E (2024) Bio-inspired preparation of silver nanoparticles on nanostructured sepiolite clay: Characterization and application as an effective adsorbent for methylene blue removal. *Inorganic Chemistry Communications* 159(1): 111786.

Gowda SA, Goveas LC and Dakshayini K (2022) Adsorption of methylene blue by silver nanoparticles synthesized from Urena lobata leaf extract: Kinetics and equilibrium analysis. *Materials Chemistry and Physics* 288(15): 126431.

Hadid M, Noukrati H, Ben Youcef H, et al. (2021) Phosphorylated cellulose for water purification: A promising material with outstanding adsorption capacity towards methylene blue. *Cellulose* 28(12): 7893–7908.

Hussain A, Li J, Wang J, et al. (2018) Hybrid monolith of graphene/TEMPO-oxidized cellulose nanofiber as mechanically robust, highly functional, and recyclable adsorbent of methylene blue dye. *Journal of Nanomaterials* 2018: 5963982.

Jedynak K and Repelewicz M (2017) Adsorption of methylene blue and malachite green on micro-mesoporous carbon materials. *Adsorption Science & Technology* 35(5–6): 499–506.

Kamel R, El-Wakil NA, Abdelkhalek AA, et al. (2020) Nanofibrillated cellulose/cyclodextrin based 3D scaffolds loaded with raloxifene hydrochloride for bone regeneration. *International Journal of Biological Macromolecules* 156: 704–716.

Kasula M, Le T, Thomsen A, et al. (2022) Silver metal organic frameworks and copper metal organic frameworks immobilized on graphene oxide for enhanced adsorption in water treatment. *Chemical Engineering Journal* 439: 135542.

Khan Z, Assad N, Naeem-ul-Hassan M, et al. (2023) Aconitum lycoctonum L.(Ranunculaceae) mediated biogenic synthesis of silver nanoparticles as potential antioxidant, anti-inflammatory, antimicrobial and antidiabetic agents. *BMC Chemistry* 17(1): 128.

Li B, Shan CL, Zhou Q, et al. (2013) Synthesis, characterization, and antibacterial activity of cross-linked chitosan-glutaraldehyde. *Marine Drugs* 11(5): 1534–1552.

Moghazy MA (2023) Leidenfrost green synthesis method for MoO3 and WO3 nanorods preparation: Characterization and methylene blue adsorption ability. *BMC Chemistry* 17(1): 1–11.

Monier M and Abdel-Latif D (2013) Synthesis and characterization of ion-imprinted resin based on carboxymethyl cellulose for selective removal of UO22 + . *Carbohydrate Polymers* 97(2): 743–752.

Monier M, Ayad D, Wei Y, et al. (2010) Adsorption of Cu (II), Co (II), and Ni (II) ions by modified magnetic chitosan chelating resin. *Journal of Hazardous Materials* 177(1–3): 962–970.

Owda ME, Elfeky AS, Abouzeid RE, et al. (2022) Enhancement of photocatalytic and biological activities of chitosan/activated carbon incorporated with TiO 2 nanoparticles. *Environmental Science and Pollution Research* 29: 18189–18201.

Pezoti O Jr, Cazetta AL, Souza IP, et al. (2014) Adsorption studies of methylene blue onto ZnCl2-activated carbon produced from buriti shells (Mauritia flexuosa L.). *Journal of Industrial and Engineering Chemistry* 20(6): 4401–4407.

Pottathara YB, Narwade VN, Bogle KA, et al. (2020) TEMPO-oxidized cellulose nanofibrils–graphene oxide composite films with improved dye adsorption properties. *Polymer Bulletin* 77: 6175–6189.

Saito T, Uematsu T, Kimura S, et al. (2011) Self-aligned integration of native cellulose nanofibrils towards producing diverse bulk materials. *Soft Matter* 7(19): 8804–8809.

Salama A (2017) Dicarboxylic cellulose decorated with silver nanoparticles as sustainable antibacterial nanocomposite material. *Environmental Nanotechnology, Monitoring & Management* 8: 228–232.

Salama A (2020) Cellulose/silk fibroin assisted calcium phosphate growth: Novel biocomposite for dye adsorption. *International Journal of Biological Macromolecules* 165: 1970–1977.

Salama A and Abou-Zeid RE (2021) Ionic chitosan/silica nanocomposite as efficient adsorbent for organic dyes. *International Journal of Biological Macromolecules* 188: 404–410.

Salama A, Abou-Zeid RE, Cruz-Maya I, et al. (2020) Soy protein hydrolysate grafted cellulose nanofibrils with bioactive signals for bone repair and regeneration. *Carbohydrate Polymers* 229: 115472.

Salama HE, Aziz MSA and Saad GR (2018) Thermal properties, crystallization and antimicrobial activity of chitosan biguanidine grafted poly (3-hydroxybutyrate) containing silver nanoparticles. *International Journal of Biological Macromolecules* 111: 19–27.

Saleh AK, El-Gendi H, El-Fakharany EM, et al. (2022) Exploitation of cantaloupe peels for bacterial cellulose production and functionalization with green synthesized copper oxide nanoparticles for diverse biological applications. *Scientific Reports* 12(1): 19241.

Saleh AK, El-Gendi H, Ray JB, et al. (2021) A low-cost effective media from starch kitchen waste for bacterial cellulose production and its application as simultaneous absorbance for methylene blue dye removal. *Biomass Conversion and Biorefinery* 13: 12437–12449.

Saleh AK, El-Gendi H, Soliman NA, et al. (2022) Bioprocess development for bacterial cellulose biosynthesis by novel lactiplantibacillus plantarum isolate along with characterization and antimicrobial assessment of fabricated membrane. *Scientific Reports* 12(1): 2181.

Saleh AK, Salama A, Badawy AS, et al. (2023) Paper sludge saccharification for batch and fed-batch production of bacterial cellulose decorated with magnetite for dye decolorization by experimental design. *Cellulose* 30: 10841–10866.

Salehi R, Arami M, Mahmoodi NM, et al. (2010) Novel biocompatible composite (chitosan–zinc oxide nanoparticle): Preparation, characterization and dye adsorption properties. *Colloids and Surfaces B: Biointerfaces* 80(1): 86–93.

Satapathy MK, Banerjee P and Das P (2015) Plant-mediated synthesis of silver-nanocomposite as novel effective azo dye adsorbent. *Applied Nanoscience* 5: 1–9.

Segal L, Creely JJ, Martin A, et al. (1959) An empirical method for estimating the degree of crystallinity of

native cellulose using the X-ray diffractometer. *Textile Research Journal* 29(10): 786–794.

Singh J and Dhaliwal A (2021) Effective removal of methylene blue dye using silver nanoparticles containing grafted polymer of guar gum/acrylic acid as novel adsorbent. *Journal of Polymers and the Environment* 29: 71–88.

Singh R, Munya V, Are VN, et al. (2021) A biocompatible, pH-sensitive, and magnetically separable superparamagnetic hydrogel nanocomposite as an efficient platform for the removal of cationic dyes in wastewater treatment. *ACS omega* 6(36): 23139–23154.

Vasylechko VO, Fedorenko VO, Gromyko OM, et al. (2017) Solid phase extractive preconcentration of silver from aqueous samples and antimicrobial properties of the clinoptilolite–ag composite. *Adsorption Science & Technology* 35(7–8): 602–611.

Vijayakumar G, Kim HJ, Jo JW, et al. (2024) Macrofungal mediated biosynthesis of silver nanoparticles and evaluation of its antibacterial and wound-healing efficacy. *International Journal of Molecular Sciences* 25(2): 861.

Wang K, Hazra RS, Ma Q, et al. (2022) Multifunctional silk fibroin/PVA bio-nanocomposite films containing TEMPO-oxidized bacterial cellulose nanofibers and silver nanoparticles. *Cellulose* 29(3): 1647–1666.

Wen X and Li J (2023) Synthesis of recyclable SERS platform based on magnetic Fe3O4/mTiO2/ag composites for photodegradation and identification of organic pollutants in different water samples. *Vibrational Spectroscopy* 129: 103600.

Wu J and Andrews MP (2020) Carboxylated cellulose nanocrystal microbeads for removal of organic dyes from wastewater: Effects of kinetics and diffusion on binding and release. *ACS Applied Nano Materials* 3(11): 11217–11228.

Xu H, Liu B and Zhang M (2023) Synthesis of silver nanoparticles composite mesoporous microspheres for synergistic adsorption-catalytic degradation of methylene blue. *Separation and Purification Technology* 324(1): 124499.

Yagub MT, Sen TK, Afroze S, et al. (2014) Dye and its removal from aqueous solution by adsorption: A review. *Advances in Colloid And Interface Science* 209: 172–184.

Yahia R, Owda ME, Abou-Zeid RE, et al. (2022) Synthesis and characterization of thermoplastic starch/PVA/cardanol oil composites loaded with in-situ silver nanoparticles. *Journal of Applied Polymer Science* 139(3): 51511.

Yang D, Liu Q, Gao Y, et al. (2023) Characterization of silver nanoparticles loaded chitosan/polyvinyl alcohol antibacterial films for food packaging. *Food Hydrocolloids* 136(B): 108305.

Yari A, Yari M, Sedaghat S, et al. (2021) Facile green preparation of nano-scale silver particles using Chenopodium botrys water extract for the removal of dyes from aqueous solution. *Journal of Nanostructure in Chemistry* 11: 423–435.

Zhang X, Gao B, Creamer AE, et al. (2017) Adsorption of VOCs onto engineered carbon materials: A review. *Journal of Hazardous Materials* 338(15): 102–123.

Zhao X, Wang X and Lou T (2022) Simultaneous adsorption for cationic and anionic dyes using chitosan/electrospun sodium alginate nanofiber composite sponges. *Carbohydrate Polymers* 276(15): 118728.